A Tampering Risk of Fiber-Based Time-Frequency Synchronization and Its Countermeasure

Hongfei Dai[1,2], Wenlin Li[1,2], Dongqi Song[1,2], Bo Wang[1,2]
[1] *State Key Laboratory of Precision Space-time Information Sensing Technology, Department of Precision Instrument, Tsinghua University, Beijing 100084, China*
[2] *Key Laboratory of Photonic Control Technology (Tsinghua University), Ministry of Education, Beijing 100084, China*
Email: bo.wang@tsinghua.edu.cn

***Abstract*—Fiber networks are utilized globally and are highly valued as effective channels for transmitting time-frequency (TF) signals. Over recent decades, considerable research has been dedicated to fiber-based TF synchronization technologies. Instruments developed from these technologies have proven effective in various applications. As these instruments become more widespread, their security issues have increasingly come to the forefront. This paper introduces a method known as the "frequency expander" to address frequency tampering. On a 200 km fiber link, we demonstrate a frequency tampering scenario using a frequency expander-enabled frequency tampering module (FTM). Additionally, we propose a hybrid fiber-based time synchronization and vibration detection method as a countermeasure. This hybrid method is exploring the idle light within the time synchronization system, i.e., Rayleigh backscattering, which is usually considered harmful.**

Keywords—Time-frequency synchronization; fiber network; frequency tampering; vibration detection.

I. INTRODUCTION

Currently, optical fiber networks are used globally and have been one of the largest infrastructure for human utilization. As an outstanding transmission medium, the optical fiber has unique advantages in transmitting time-frequency (TF) references [1]. For several decades, the development and study of TF synchronization methods utilizing optical fibers have been a focal area of research [2]. Instruments derived from these methods have been effectively utilized across various sectors, including metrology, telecommunications, navigation, and radio astronomy. In the future, it is anticipated that fiber-based TF synchronization instruments will fulfill the rigorous timing demands essential in areas such as fifth and sixth generation communications, smart urban development, global seismic observation, and distributed computing systems [3], [4].

As the deployment of fiber-based time-frequency (TF) synchronization instruments expands, their security has become an important issue that must be considered in advance. However, current research on their security remains insufficient. Notably, there are limited studies specifically addressing the risks associated with frequency synchronization. Moreover, present TF synchronization systems lack direct methods for detecting risky behaviors. These shortcomings present potential risks for the large-scale deployment of fiber-based TF synchronization instruments.

In this paper, we propose a frequency tampering method called "frequency expander" to reveal a risk of fiber-based frequency synchronization (FbFS) systems [5]. A frequency expander-enabled frequency tampering module (FTM) can be covertly inserted into a fiber link at any arbitrary point. It can controllably change the value of a disseminated frequency without compromising the relative stability of the frequency dissemination and bypassing the phase-locking status monitoring. In our case, tampering with the recovered 100 MHz signal within ±100 Hz is demonstrated on a 200 km fiber link. The relative stability of the recovered frequency is maintained at the same level as the original state.

Additionally, this paper proposes a hybrid fiber-based time synchronization (FbTS) and vibration detection method as a countermeasure [6]. Central to this hybrid method is exploring the idle light within the time synchronization system, i.e., Rayleigh backscattering, which is usually considered harmful to time synchronization. By analyzing the phase fluctuation of this idle light, we can detect vibrations along the fiber link without impacting the performance of FbTS. This system not only accurately identifies vibrations but also pinpoints their timing and location, effectively equipping the TF synchronization network with an intrinsic safety monitoring feature.

II. METHODS/RESULTS

A. Principle of frequency expander-enabled FTM

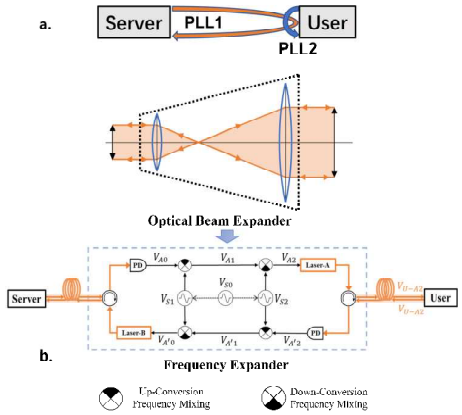

Fig. 1. Principles of FbFS and the frequency expander-enabled FTM. (a) Structure of a typical FbFS system. (b) Comparison between the optical beam expander and the frequency expander. PLL, phase-locked loop [5].

A conventional fiber-based radio frequency synchronization system, shown in Fig. 1(a), is generally made up of two phase-locked loops (PLLs), namely PLL1 and PLL2. PLL1 is employed to counteract noise fluctuations within the link, and PLL2 focuses on enhancing the phase noise of the recovered signal at the user end. If an intruder tries to disrupt the synchronization process by tampering with the recovered frequency, it impacts the locking condition of PLL1. However,

This work was supported in part by the National Natural Science Foundation of China under Grant 62171249, in part by the National Key Project of Research and Development under Grant 2021YFA1402102, and in part by Tsinghua Initiative Scientific Research Program.

if the tampering can evade the monitoring of the locking status, it allows for the subtle and clandestine modification of the recovered frequency.

We employ a "frequency expander" to achieve covert tampering. This concept draws inspiration from the optical beam expander. According to the reversibility principle in geometrical optics, light will trace the same path if its direction is reversed. A beam expander, comprising two lenses, can either broaden or narrow the beam width, as illustrated in Fig. 1(b). When the broadened (or narrowed) beam travels in the reverse direction through the beam expander, it restores the beam width to its original dimension. Similarly, if the disseminated frequency signal can be altered in this manner, stealthy frequency tampering becomes possible. As depicted in Fig. 1(b), the frequency expander can augment (or reduce) the frequency of the transmitted signal. When the output frequency signal traverses the frequency expander in the reverse direction, it can revert the frequency to its initial state. This also allows for the circumvention of locking status monitoring. Fig. 1(b) provides a detailed schematic of the frequency expander-enabled FTM. There is an oscillator V_{S0}, i.e., $V_{S0} = cos(2\pi f_{S0}t + \phi_{S0})$ The signals V_{S1} and V_{S2} are synthesized via V_{S0}, as follows:

$$V_{S1} = \cos[2\pi(k + k_1)f_{S0}t + (k + k_1)\phi_{S0}], \quad (1)$$

$$V_{S2} = \cos(2\pi k f_{S0}t + k\phi_{S0}), \quad (2)$$

where k and k_1 are the frequency synthesis factors. Compared with k, the factor k_1 is very small, which is usually smaller than 2.1×10^{-4}.

With the frequency expander-enabled FTM, the input signal V_{A0} (the disseminated RF signal modulated on the laser carrier, i.e., $V_{A0} = \cos(2\pi f_{A0}t + \phi_{A0})$), can be converted parametrically to the output signal V_{A2} in the forward direction. Conversely, in the backward direction, the signal $V_{A'2}$ (the same frequency as V_{A2}) can be parametrically converted to the signal $V_{A'0}$ again (the same frequency as V_{A0}). Specifically, the parametrical conversion process is accomplished by using second-order nonlinear electronic devices, such as RF mixers, to generate signals V_{A1} and V_{A2}. In the forward direction, V_{A1} is generated by up-mixing V_{A0} and V_{S1}, while V_{A2} is generated by down-mixing V_{A1} and V_{S2}, as follows:

$$V_{A1} = \cos\{2\pi[(k + k_1)f_{S0} + f_{A0}]t + (k + k_1)\phi_{S0} + \phi_{A0}\}, \quad (3)$$

$$V_{A2} = \cos[2\pi(k_1 f_{S0} + f_{A0})t + k_1\phi_{S0} + \phi_{A0}]. \quad (4)$$

Consequently, the disseminated frequency is shifted from f_{A0} to $(k_1 f_{S0} + f_{A0})$. The output signal V_{A2} can be used to modulate the laser carrier again, which is transmitted to the user site along the optical fiber link. Referring to Appendix A, the RF signal V_{U-A2} is recovered at the user side, i.e., $V_{U-A2} = \cos[2\pi(k_1 f_{S0} + f_{A0})t + k_1\phi_{S0} + \phi_{A0} + \phi_{n2}]$, where ϕ_{n2} is the phase noise introduced by this part of the fiber link between the FTM and the user site.

At the user site, the RF signal V_{U-A2} is also modulated on another laser carrier, whose wavelength is different, and returned to the FTM along the fiber. In the backward direction, signal $V_{A'2}$ is detected by the FTM, as follows:

$$V_{A'2} = \cos[2\pi(k_1 f_{S0} + f_{A0})t + k_1\phi_{S0} + \phi_{A0} + 2\phi_{n2}]. \quad (5)$$

In the lower part of the FTM, $V_{A'0}$ can be obtained by similar treatments in (3) and (4), as follows:

$$V_{A'0} = \cos(2\pi f_{A0}t + \phi_{A0} + 2\phi_{n2}). \quad (6)$$

In this manner, we achieve symmetrical enlargement and reduction of the disseminated frequency, such as $f_{A0} \rightarrow f_{A2}$ and $f_{A'2} \rightarrow f_{A'0}$. Considering the relationship between $f_{A0} = f_{A'0}$ and $f_{A2} = f_{A'2}$, the inclusion of the FTM does not interfere with the normal functioning of the frequency synchronization system. Essentially, the disseminated frequency can be modified by making slight adjustments to the parameter k_1, while still maintaining the locking status.

B. Frequency tampering experiment on a 200-km fiber link

As illustrated in Fig. 2, we have developed a fiber-based radio frequency synchronization system. This system includes a server and a user, connected via a 200-km fiber link. The server is synchronized to a 100 MHz output from a hydrogen maser. To enable frequency tampering, we integrate the FTM into the fiber link, as depicted in Fig. 2.

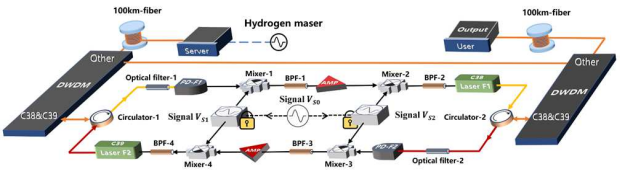

Fig. 2. Schematic diagram of the frequency expander-enabled FTM. Orange lines indicate optical fiber links, while the black line represents RF signals. DWDM, dense wavelength division multiplexing; PD, photodetector; BPF, band-pass filter; AMP, amplifier [5].

This FTM is composed of two dense wavelength division multiplexing (DWDM) modules, two optical switches, a short fiber connected to the 'other' ports of DWDM modules, and the key part of the FTM connected to the C38/C39 ports of DWDM modules. Inside the FTM, the optical signals from both directions are detected by photodetectors (PDs). A 10 MHz oscillator V_{S0} is used to synthesize the signals V_{S1} and V_{S2} as shown in (1) and (2), where $k = 90$, and k_1 can be set within $\pm 2.1 \times 10^{-4}$. Specifically, in the experiment, f_{S1} is set to $(900 + 10k_1)$ MHz, and f_{S2} is set to 900 MHz. k_1 is the key to achieving frequency tampering, and k is also selected to avoid harmonic interference in the frequency mixing process. Based on our experimental system, we obtain the frequency f_U recovered by the user which satisfies the following equation:

$$f_U = \left(100 + \frac{10k_1}{21}\right) MHz. \quad (7)$$

Next, we further investigate the effect of the FTM on frequency dissemination stability. We select three different values of k_1 to set the corresponding recovered frequency f_U to 100 MHz+1 Hz, 100 MHz+10 Hz, and 100 MHz+100 Hz. As a comparison, under the same experimental conditions, we also measure the relative stability between the recovered frequency signal at the user end and the frequency reference at the server end without the FTM insertion. The experimental results are shown in Fig. 3. The equipment we use to measure frequency stability is the phase noise and Allen deviation tester, Microsemi, 5125A. When the FTM is not added to the fiber link, relative stability results are $1.6 \times 10^{-14}/1$ s and $2.1 \times 10^{-17}/10^4$ s. When the FTM is added, the relative stability results under three different values of k_1 remain at $2.2 \times 10^{-14}/1$ s and $2.2 \sim 3.0 \times 10^{-17}/10^4$ s. Thus, the insertion of the FTM has little effect on the frequency

dissemination stability and the relative stability of the recovery signal is also almost the same when k_1 takes different values.

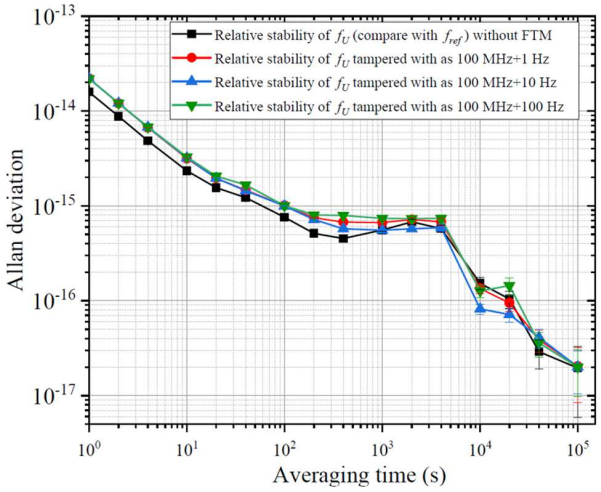

Fig. 3. Relative stability of the recovered frequency signal under the different parameter settings of the FTM. With the FTM, f_U is altered to 100 MHz+1 Hz, 100 MHz+10 Hz, and 100 MHz+100 Hz, respectively. A comparison is made with the scenario without FTM insertion [5].

C. *Principle of the hybrid FbTS and vibration detection system*

The principle of FbTS method we utilized, i.e., time reversal enabled FbTS, which are shown in Fig. 4(a), can be found in [7]. This method eliminates the need for data transmission between the server and users, as well as the measurement of fiber transfer delay. In the FbTS system, if optical carriers with the same wavelength are used, the Rayleigh backscattering generated by time pulses can degrade the signal-to-noise ratio (SNR) of time interval measurements, thereby affecting the performance of FbTS. To prevent this, optical carriers with different wavelengths, i.e., λ_s and λ_u, are employed to avoid this effect. In this way, the Rayleigh backscattering, i.e., L_{i_k}, becomes the idle pulse. Although it is a by-product and useless for FbTS system, it is valuable for vibration detection.

Above all, the vibration detection is realized at user site, as shown in Fig. 4(b). The laser pulse modulated by the clock signal t_{u_k} generates Rayleigh scattering L_{i_k} during transmission. The repetition rate of the laser pulse is f_c. The pulse width of t_{u_k} is set to be T_w, which corresponds to the vibration sensing gauge length of L_G, i.e.,

$$L_G = T_w \frac{c}{n}, \tag{8}$$

where c is the speed of light in the vacuum, and n is the refractive index of the fiber. It means that the whole fiber is divided into many sensing channels. The location of channel j, i.e. x_j, can be identified by the round-trip time delay, i.e.,

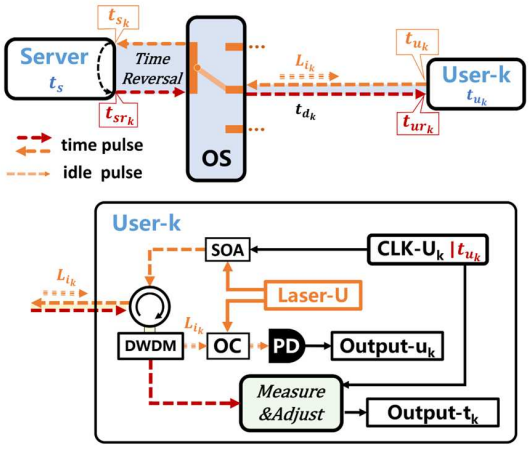

Fig. 4. (a) Principle diagram of multi-user time synchronization based on the fiber network. (b) More details of User-k. SOA: semiconductor optical amplifier; DWDM: dense wavelength division multiplexing; OS: optical switch; OC: optical coupler; PD: photodetector [6].

$$x_j = \frac{t_j c}{2n}, \tag{9}$$

where t_j is the round-trip delay. An optical interferometer is set up at User-k. After interference between L_{i_k} and Laser-U, $output - u_k$ is obtained. Coherent backscattered pulse at the location x_j of fiber has a predictable phase, which can be represented by $\phi_{output-u_k}(x_j)$:

$$\phi_{output-u_k}(x_j) = \frac{4\pi n x_j}{\lambda_u}. \tag{10}$$

Vibrations in the fiber cause strain, altering $\phi_{output-u_k}(x_j)$. The phase change $\Delta\phi_{output-u_k}$ can be expressed as:

$$\Delta\phi_{output-u_k}(x_j) = \frac{4\pi n \cdot \Delta x_j}{\lambda_u} = \frac{4\pi n L_G \varepsilon_{x_j}}{\lambda_u}, \tag{11}$$

where ε_{x_j} is the strain happened at x_j. Consequently, the strain at x_j can be described as,

$$\varepsilon_{x_j} = \frac{\Delta\phi_{output-u_k}(x_j)\lambda_u}{4\pi n L_G}. \tag{12}$$

D. *Experiments in multi-user time synchronisation and vibration detection*

For the experimental setup, we selected two users, User-1 and User-2, for demonstration purposes. Both users have identical configurations. User-1 is connected to the server via a 35-km fiber (Link-1), and User-2 is connected via a 40-km fiber (Link-2). The fibers used in the experiment are of type G652.D, with a refractive index of n=1.467.

In time synchronization tests, the time difference between CLK-S and $output - t_k$, whose repetition rates both are 1 kHz, is measured by a time interval counter (model 53230A, Keysight). TDEV results are shown in Fig. 5. For time synchronization between User-1 and the Server, TDEV results are 3.5 ps at $\tau = 1$ s and 1.0 ps at $\tau = 10^4$ s. For time synchronization between User-2 and the Server, TDEV results are 3.6 ps at $\tau = 1$ s and 1.4 ps at $\tau = 10^4$ s.

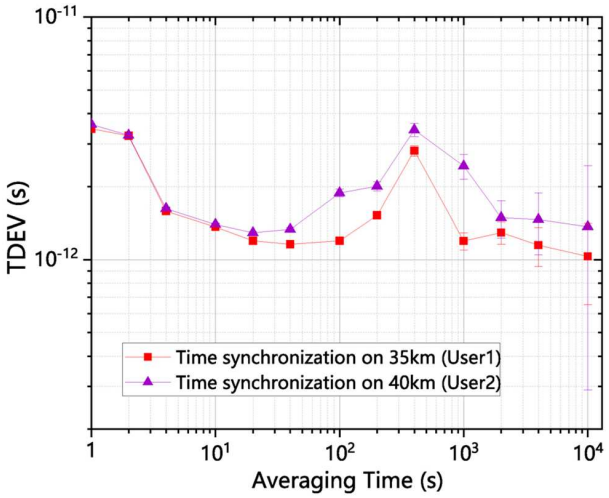

Fig. 5. Time deviation (TDEV) results for different users [6].

To demonstrate its vibration-detection capability, a 20 Hz sinusoidal signal is applied to FS-1, and a 10 Hz sinusoidal signal is applied to FS-2 at different times. As previously mentioned, the time pulse repetition rate is 1 kHz. The laser pulse scans the entire fiber link at this frequency. According to the Nyquist theorem, the system can detect vibrations with frequencies up to 500 Hz. Based on (12), the phase fluctuation of $output - u_k$ is converted to the strain of the fiber link, i.e., ε_{x_j}. The vibration-detection results are presented in Fig. 6.

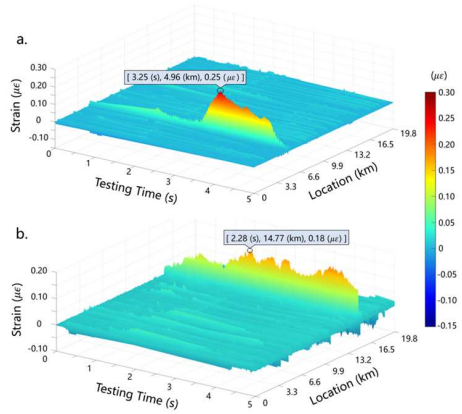

Fig. 6. Detection results of vibrations on Link-1 and Link-2. (a) Detection results on Link-1. (b) Detection results on Link-2 [6].

On Link-1, a significant vibration is detected approximately 4.96 km away from User-1. The peak axial strain resulting from this vibration reaches 0.25 $\mu\varepsilon$. On Link-2, there is also a notable vibration identified around 14.77 km from User-2. The peak axial strain resulting from this vibration reaches 0.18 $\mu\varepsilon$. This test demonstrates the capabilities of the system to detect and localize vibrations along the fiber links.

III. Conclusion

We show that the synchronized frequency reference can be modified using a frequency expander-enabled FTM on a 200 km fiber link. By circumventing the locking status monitoring, the 100 MHz frequency reference synchronized at the user end can be discreetly and arbitrarily altered within a range of 100 MHz±100 Hz. Additionally, the relative stability of the tampered frequency reference remains consistent with its normal level. Furthermore, we propose a hybrid method for time synchronization and vibration detection based on fiber. This method integrates multiple functionalities by repurposing idle pulses, specifically the Rayleigh backscattering generated during time synchronization, thus converting what would be waste into a useful resource for detecting vibrations. Importantly, this does not compromise the time synchronization performance. The system is also capable of accurately identifying and locating abnormal vibrations along the link, potentially providing a solution for enhancing link security.

References

[1] B. Wang, C. Gao, W. L. Chen, J. Miao, X. Zhu, Y. Bai, J. W. Zhang, Y. Y. Feng, T. C. Li, and L. J. Wang, "Precise and continuous time and frequency synchronisation at the 5×10^{-19} Accuracy Level," Sci. Rep., vol. 2, p. 556, 2012.

[2] F. Riehle, "Optical clock networks," Nat. Photonics, vol. 11, no. 1, pp. 25–31, 2017.

[3] Y. He, K. G. H. Baldwin, B. J. Orr, R. Bruce Warrington, M. J. Wouters, A. N. Luiten, P. Mirtschin, T. Tzioumis, C. Phillips, J. Stevens, B. Lennon, S. Munting, G. Aben, T. Newlands, and T. Rayner, "Long-distance telecom-fiber transfer of a radio-frequency reference for radio astronomy," Optica, vol. 5, pp. 138–146, 2018.

[4] M. Schioppo, J. Kronjaeger, A. Silva, R. Ilieva, J. Paterson, C. Baynham, W. Bowden, I. Hill, R. Hobson, A. Vianello et al., "Comparing ultrastable lasers at 7×10^{-17} fractional frequency instability through a 2220 km optical fibre network," Nat. Commun., vol. 13, no. 1, p. 212, 2022.

[5] H. Dai, Y. Chen, W. Li, F. Wang, G. Wang, Z. Pang, C. Li, and B. Wang, "A Tampering Risk of Fiber-Based Frequency Synchronization Networks," IEEE Trans. Instrum. Meas, doi: 10.1109/TIM.2024.3414551.

[6] H. Dai, D. Song, W. Li, G. Wang, Z. Pang, C. Li, and B. Wang, "Hybrid Fiber-Based Time Synchronization and Vibration Detection System," Opt. Lett., vol. 49, pp. 3372-3375, 2024.

[7] Y. Chen, H. Dai, W. Li, F. Wang, B. Wang and L. Wang, "Time Reversal Enabled Fiber-Optic Time Synchronization," IEEE Trans. Instrum. Meas, vol. 72, 5503508, 2023.